Available online at www.sciencedirect.com

SciVerse ScienceDirect

Journal of the European Ceramic Society 32 (2012) 2519–2527

www.elsevier.com/locate/jeurceramsoc

High-temperature bending strength, internal friction and stiffness of ZrB_2–20 vol% SiC ceramics

Ji Zou [a,b,c], Guo-Jun Zhang [a,*], Chun-Feng Hu [b], Toshiyuki Nishimura [b], Yoshio Sakka [b,*], Hidehiko Tanaka [b], Jef Vleugels [c,*], Omer Van der Biest [c]

[a] State Key Laboratory of High Performance Ceramics and Superfine Microstructures, Shanghai Institute of Ceramics, Shanghai 200050, China
[b] National Institute for Materials Science NIMS, 1-2-1 Sengen, Tsukuba, Ibaraki 305-0047, Japan
[c] Department of Metallurgy and Materials Engineering (MTM), Katholieke Universiteit Leuven, B-3001 Heverlee, Belgium

Received 21 September 2011; received in revised form 22 January 2012; accepted 26 January 2012
Available online 4 March 2012

Abstract

Dense ZrB_2–20 vol% SiC ceramics (ZS) were fabricated by hot pressing using self-synthesized high purity ZrB_2 and commercial SiC powders as raw materials. The high temperature flexural strength of ZS and its degradation mechanisms up to 1600 °C in high purity argon were investigated. According to the fracture mode, crack origin and internal friction curve of ZS ceramics, its strength degradation above 1000 °C is considered to result from a combination of phenomena such as grain boundary softening, grain sliding and the formation of cavitations and cracks around the SiC grains on the tensile side of the specimens. The ZS material at 1600 °C remains 84% of its strength at room temperature, which is obviously higher than the values reported in literature. The benefit is mainly derived from the high purity of the ZrB_2 powders.

Keywords: ZrB_2–SiC; UHTCs; High temperature strength; Internal friction; Crack origin; Grain sliding

1. Introduction

ZrB_2 is one of the ultra-high temperature ceramics (UHTCs), which are of considerable interest for applications that require exposure to extreme thermal and chemical environments such as the leading edge components and thermal protection systems in future hypersonic aerospace vehicles (7–20 Mach).[1–3] In order to improve the oxidation resistance and mechanical properties of ZrB_2, silicon carbide (SiC) is commonly used as an additive. ZrB_2–20 vol% SiC particulate composite (ZS) is regarded as the baseline materials in this research.

The densification process,[4–6] microstructure tailoring,[7–9] oxidation/ablation resistance,[1,10,11] thermo-physical[12] and mechanical properties of ZrB_2–SiC composites[13] have been extensively investigated in the last 10 years. The flexure strength of ZrB_2–SiC ceramics at elevated temperatures is an important factor for the applications in the extreme environment. However, there lack data of the high temperature flexure strength and fracture behavior of ZrB_2–SiC composites.

A number of previous studies[14,15] only reported some strength values of ZS material at a limited range of temperatures, but strength degradation mechanisms are not available; Bellosi et al. evaluated the strengths of ZrB_2–10 vol% SiC ceramics fabricated from commercial ZrB_2 and SiC powders with or without ZrC additions at 1500 °C in argon or air atmosphere. The results indicated that the loss of strength of the ZrB_2–10 vol% SiC ceramics was not obvious when the samples sintered by Spark Plasma Sintering (SPS). The favorable effects were mainly attributed to the clean grain boundaries in the as-SPSed samples.[16] However, their samples in the experiments were partially oxidized during the measurements. In addition, Hu[17] reported that the flexure strengths and behavior of ZrB_2 with 15 vol% and 30 vol% SiC additions at 1800 °C were controlled by the ZrB_2 and SiC grain sizes in the ZrB_2–SiC particulate composites. The fracture strength of the ZrB_2–15 vol% SiC composites at 1800 °C decreased from 217 MPa for coarse

* Corresponding authors.
E-mail addresses: gjzhang@mail.sic.ac.cn (G.-J. Zhang), SAKKA.Yoshio@nims.go.jp (Y. Sakka), Jozef.Vleugels@mtm.kuleuven.be (J. Vleugels).

0955-2219/$ – see front matter © 2012 Elsevier Ltd. All rights reserved.
doi:10.1016/j.jeurceramsoc.2012.01.035

grains (ZrB_2 5 μm, SiC 2 μm) and to 112 MPa for fine grains (ZrB_2 2 μm, SiC 0.5 μm), and meanwhile the fracture behavior transformed from elastic fracture to plastic deformation. In Hu's studies, the authors only reported the fracture strengths at room temperature and 1800 °C, and did not offer any data concerning the temperature dependence of strength and strength degradation mechanisms.

Softening of grain boundary at elevated temperatures leads to strength degradation of ceramics, especially when low melting point phases exist at the grain boundaries. In order to minimize the grain boundary phases with low melting point and improve the high temperature strengths of ZS material, high purity ZrB_2 powders synthesized through a carbon-thermal/boron-thermal reduction method were used in the present research. The bending strength and Young's modulus (E) of ZS material at various temperatures were measured in a high purity argon atmosphere, i.e. the tested bars almost would not be oxidized. The effect of grain boundary characters on the strength loss at elevated temperatures was studied by high-resolution transmission electron microscopy (HRTEM) observations together with internal friction analysis. The strength degradation mechanisms of ZS were comprehensively investigated and discussed.

2. Experimental procedure

The ZrB_2 powder was synthesized by the reaction between ZrO_2 and B_4C at 1600 °C in vacuum. A similar synthesis procedure could be found as for HfB_2 powder.[18] The crystalline phase, impurities content, average particle size and suppliers of ZrB_2 and SiC powders are listed in Table 1. Apart from Hf, the total impurities (0.6 wt%) and the oxygen content (0.5 wt%) in the as synthesized ZrB_2 powder are obviously lower than those in commercial ZrB_2 powders.[12,16,17] Furthermore, the carbon content in ZrB_2 powders is as low as 0.10 wt%, i.e. the residual boron carbide in the as-synthesized ZrB_2 powder is limited. The ZrB_2 and SiC powders were mixed with acetone in a resin jar for 12 h using Si_3N_4 media. Then the slurry was dried and sieved. The compacts of the mixed raw powders were hot pressed at 2000 °C and at 30 MPa for 1 h in a flowing argon atmosphere. The processing details and densification procedures have been reported in our previous reports.[19]

Three-point bending tests were performed at temperatures in the range from ambient temperature to 1600 °C and at the crosshead speed of 0.5 mm/min. The dimension of the specimens was 2 mm × 2.5 mm × 25 mm (thickness × width × length). The tensile surfaces of the specimens were polished to a 1.5 μm diamond finish and chamfered. Then, the polished specimens were placed on a graphite bend ring in a furnace equipped with tungsten mesh heating elements. The total pressure in the furnace was vacuumed to $<10^{-3}$ Pa by a diffusion pump, followed by introducing high purity argon (>99.999%) at flowing rate of 100 ml/min to keep a high oxygen-free environment in the furnace and to prevent the test bars from oxidation during measurements. The bars were soaked at the testing temperatures for 20 min to reach a thermal equilibrium. The reported flexure strengths are the average of five specimens at room temperature and of three specimens at high temperatures. The microstructures of ZS before and after testing were observed by scanning electron microscopy (SEM, TM3000, Hitachi, Japan) and HRTEM (JEM 2100, JEOL, Japan) equipped with an X-ray energy dispersive detector systems (EDS, Model Link-ISIS, Oxford Instruments, UK).

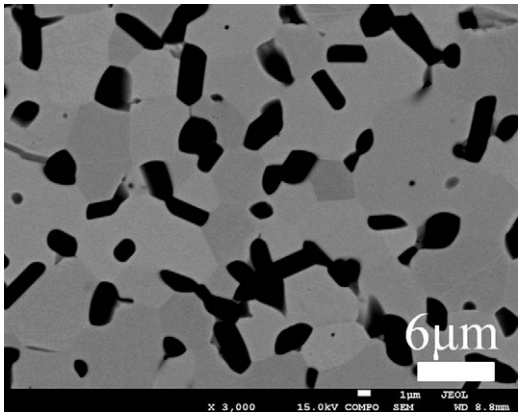

Fig. 1. Microstructure of ZrB_2–20% SiC ceramics hot pressed sintered at 2000 °C for 1 h in argon.

The Young's modulus (E) and internal friction (Q^{-1}) of the ZS specimens with the dimension of 5 mm × 1.5 mm × 40 mm were measured by an impulse excitation technique (HTVP-1750-C, IMCE, Diepenbeek, Belgium) in argon atmosphere at temperatures from 25 °C to 1300 °C with a heating rate of 2 °C/min as previously described.[20,21]

3. Results and discussions

3.1. General microstructure

The microphotograph of ZS shown in Fig. 1 indicates that the average particle size of ZrB_2 grains is 6.1 ± 1.4 μm, plate-like SiC grains with the average length of 5.3 ± 2.1 μm and width of 1.1 ± 0.8 μm are homogenously dispersed in the ZrB_2 matrix. It should be noted that the color contrasts of some small regions are different from those of ZrB_2 and SiC. It is very hard to identify these phases simply by SEM. According to the detailed microstructural analysis of ZS material conducted by TEM, two secondary phases have been found, and the representative ones are shown in Fig. 2. The first is crystallized hexagonal boron nitride (Fig. 2a), the other one with the composition of Zr–Ca–(Al)–Si–O (Fig. 2b and c, sometimes Al could not be detected from EDS) is an amorphous phase, as confirmed by its electronic diffraction pattern (Fig. 2d). The formation of BN should result from the reaction between B_2O_3 (from starting powders) and Si_3N_4 (incorporated with the milling balls) through reaction (I),[22] while the Zr–Ca–(Al)–Si–O phase presumably comes from the impurities in the starting powders as well as the milling balls (Si_3N_4 with CaO and Al_2O_3 additions). However, these impurities are very difficult to find during TEM observation, indicating that their amounts in ZS ceramics are extremely low, which is in accordance with the element content analysis of ZrB_2 and SiC powders.

$$2B_2O_3 + Si_3N_4 = 4BN + 3SiO_2 \quad \text{(I)}$$

Table 1
Characteristics of the raw materials.

Powders	Particle size (D_{50})	Impurities (%)	Supplier
Received ZrB_2	1.05 μm	O 0.46, C 0.1, Hf 1.10, Fe 0.084, Ca 0.06, Ti 0.016, others < 0.01	Self-synthesized
α-SiC	0.45 μm	B 0.33, O 1, Ca 0.24, C*l* 0.1, Fe 0.16, V 0.09	Changle Xinyuan Carborundum Co. Ltd.

The HRTEM analysis also reveals that all observed ZrB_2/SiC and ZrB_2/ZrB_2 grain boundaries are very clean (Fig. 3a and b). In addition, stress patterns with bright/dark alternating contrasts (Fig. 3a) and stacking faults (Fig. 3c) were always observed in SiC grains. The formation of stress patterns is thought to be associated with the residual compressive stress in the SiC grains, which is generated during the cooling process, due to the difference of the thermal expansion coefficient between SiC (4.5×10^{-6}/°C) and ZrB_2 (6.8×10^{-6}/°C).[12,23]

3.2. High temperature bending strengths

Three-point bending strengths of ZS as a function of test temperatures are shown in Fig. 4a. It is interesting to note that the strength of ZS is 24% higher at 1000 °C (677 MPa) compared with that measured at room temperature (546 MPa). Imperfect surface defects induced by machining, as preexisting flaws, always exist on the surface of ceramic material. Such strength improvement is probably related to the crack healing on the tensile surfaces of bars during the high temperature test, which often occurs in other structural ceramics.[24] When the test temperature was higher than 1000 °C, the strength of ZS decreased linearly with temperatures up to 1600 °C. At 1400 °C, ZS material still maintained almost 100% strength as tested at room temperature and at 1600 °C this percentage dropped to 84%. These results are obviously higher than the data reported by Loehman[14] (48%, 1400 °C) and Rhodes[15] (83%, 1400 °C), i.e. the high temperature bending strength of ZS composites sintered from self-synthesized ZrB_2 powders shows definite superiority compared to that sintered from commercial powders.

It is well known that the degradation of flexure strength of ceramics at elevated temperature always relates to the softening of grain boundary or softening secondary phase.[25,26] This viewpoint has also been cited to support the rapid fall-off in strength of ZrB_2–SiC ceramics above 1100 °C in Loehman's work,[14] since glass phases with compositions of Mg–Al–Si–Zr–Ca–O were always observed at ZrB_2/ZrB_2 and ZrB_2/SiC grain boundaries in their samples. So the relatively higher elevated temperature strengths of ZS material in the present work should result from

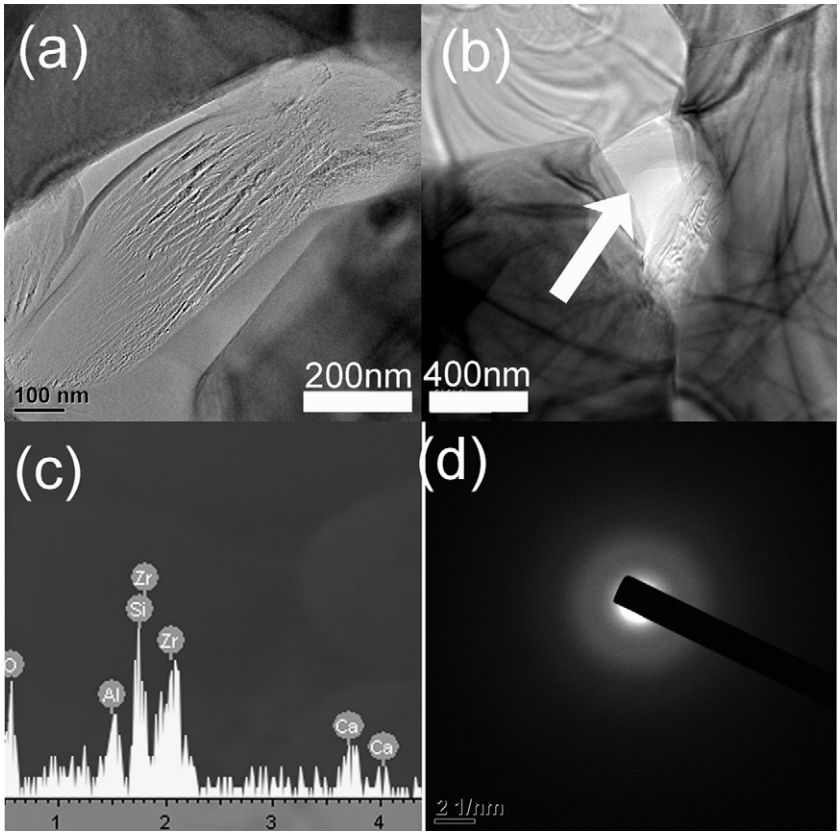

Fig. 2. The impurity phases in ZS ceramics observed by TEM, (a) hexagonal BN, (b) Zr–Ca–(Al)–Si–O based amorphous phase. (c) and (d) is the corresponding EDS and ED patterns of the area marked in (b).

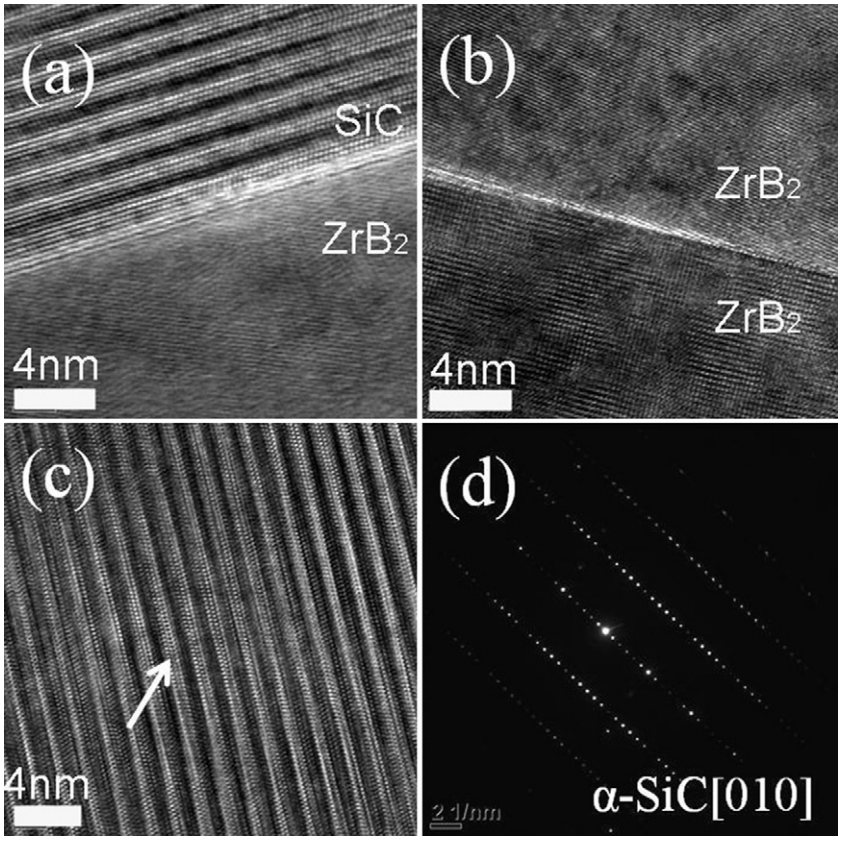

Fig. 3. HRTEM images showing ZrB_2/SiC (a) and ZrB_2/ZrB_2 (b) grain boundaries in ZS. The stacking faults in SiC grains in ZS and corresponding electron diffraction are shown in c and d, respectively.

the limited amount of glass phases in their microstructures. However, as shown in Fig. 4a, gradual decrease in strength was still observed above 1000 °C. In order to gain an insight into the strength degradation mechanisms of ZS ceramics with the increase of temperature, the fracture surface of ZS specimens tested at different temperatures were investigated.

3.3. Fracture mode

SEM analysis of the fracture surfaces of ZS tested at different temperatures clearly revealed the directions of crack propagation, as marked in their tensile surface (Fig. 5a, d, g and h). Furthermore, according to the load–displacement curves of ZS (Fig. 4b), no detectable deviations from linearity up to the facture point were observed even at 1600 °C. Both support that ZS ceramics fractured in a brittle mode from 25 °C to 1600 °C. Using high purity ZrB_2 powders as raw materials, the brittle-to-ductile transition temperature (BDTT) of ZS composites could be increased to 1600 °C or higher.

Both ZrB_2 and SiC grains in ZS specimens failed in a predominantly transgranular manner at room temperature after the bend test (Fig. 5b and c). The fracture surfaces of ZS remained almost unchanged when test temperature was elevated to 1000 °C (Fig. 5e and f). However, with a further increase of test temperature to 1300 °C or above, SEM pictures showed that the fracture mode of ZS material gradually changed from

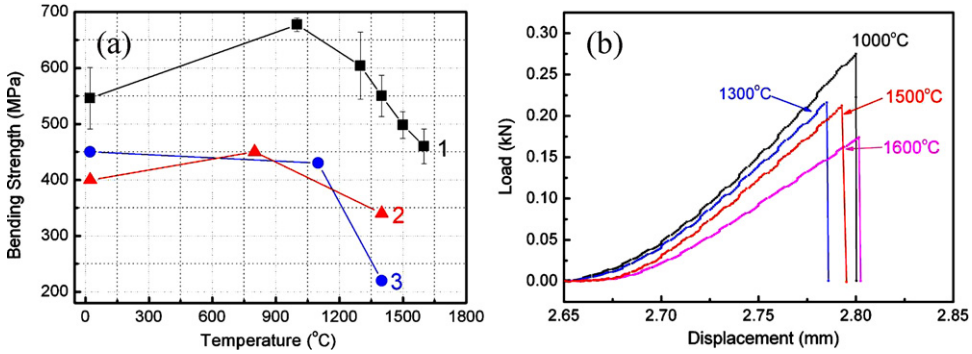

Fig. 4. (a) Temperature dependence of bend strength for ZS (1), 2 and 3 were got from Rhodes and Loehman's work, respectively. (b) The load–displacement curves for ZS at different temperatures.

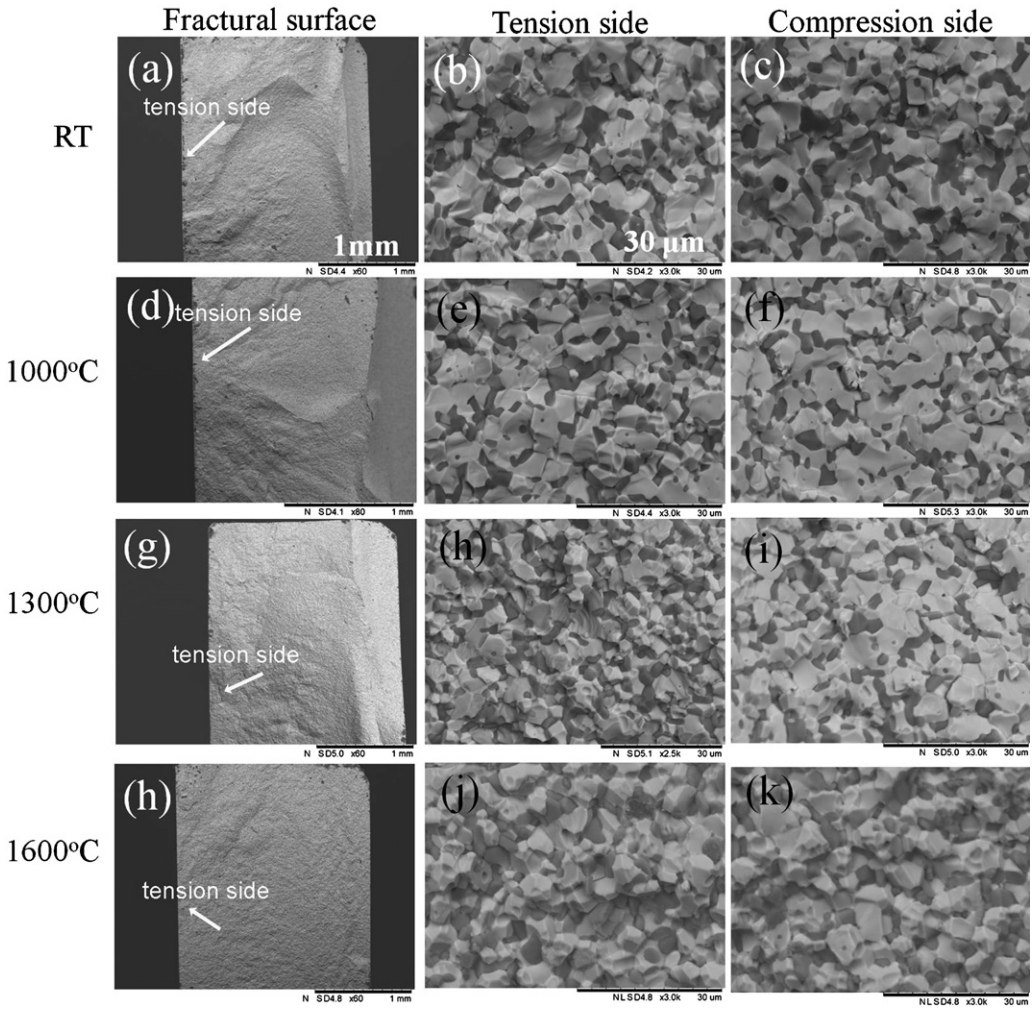

Fig. 5. The fractural surfaces of ZS at different temperatures. Test temperatures, tension or compression sides have been marked. The scales in (a), (d), (g) and (h) are the same; the others are the same with the scale marked in b.

transgranular to intergranular manner (Fig. 5h and j). Moreover, this process is companied with a decrease in strength of ZS from 546 ± 55 MPa at 25 °C to 460 ± 31 MPa at 1600 °C. What is more, such conversion in fracture mode of ZrB_2 and SiC grains was easier to occur in tensile side of the testing bars compared to that in compressive side, for example, at 1300 °C, intergranular fracture was predominant at the tensile side of the specimens (Fig. 5h) whereas most of their grains still kept transgranular fracture behavior at the compressive side (Fig. 5i).

The differences between transgranular strength (TS) and intergranular strength (IS) are the most important factor to determine the fracture mode of testing bars. At 25 °C, ZS exhibited a predominantly transgranular fracture behavior since IS is higher than TS. With the increasing of temperatures, both IS and TS decreased, but IS usually decreased more quickly than TS. This is one of the reasons for the fracture mode conversion in ZS at high temperatures. As we know, the stress acting at the crack tip in the "compressive side" is not compression but tension. Transgranular fracture mode still observed in the "compressive side" at 1300 °C is owned to the sufficiently large kinetic energy of the material around the crack that has moved distantly from the fracture initiation site.

3.4. Fracture origins

According to Griffith criterion, the fracture of brittle ceramics results from the propagation of a critical crack. The size of critical crack is one of the governing factors to determine the fracture strength of ceramics, so the source of critical crack and its initiation stage are very important to understand the fracture mechanisms of ZS at different temperatures. As discussed in Section 3.2, both SEM pictures (Fig. 5a) and literature reports[24] support that the critical crack below 1000 °C come from the imperfect surface finishes of ZS, since a clear fracture mirror, mist and hackle region originating from a surface flaw can be observed (Fig. 5a). The healing process of these flaws during high temperature test is helpful to improve the strength of ZS at 1000 °C. With the continuous increase in temperature to 1600 °C, more and more machining induced flaws should be healed. On the contrary, the strength of ZS decreased. So it is reasonable to assume that the fracture initiation of ZS has been changed. A more clear proof of such phenomena is that SEM analysis of the fracture surface revealed large surface defect on the tensile surface of ZS fractured at 25 °C (arrowed in Fig. 6a), but not found at 1000 °C (Fig. 6b).

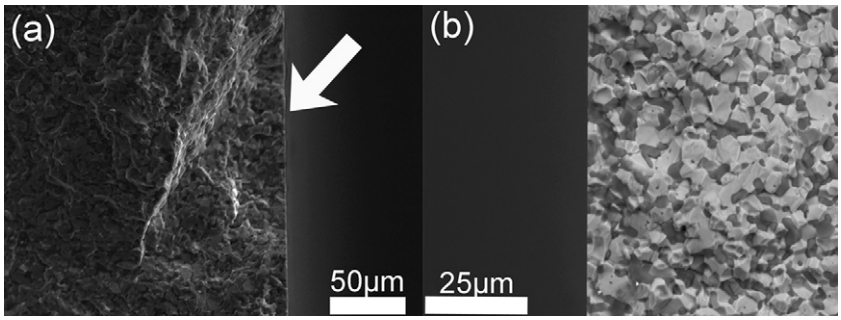

Fig. 6. SEM images show the fracture origin of ZS ceramics at room temperature (a) and 1000 °C (b) with a high magnification.

Fig. 7 shows the representative domains on the polished tensile surface of ZS bars tested at 1300 °C and 1600 °C. Examination of the sections near the fracture parts where the maximum stress was applied (Fig. 7a and c) revealed that cavities were formed. These cavities were mostly located at the triple points of SiC or the triple points among SiC and ZrB_2 grains (Fig. 7e). Furthermore, it was found that there were no pores present at the regions of the specimens without stress applied (e.g., at edge of the bars, Fig. 7b and d), suggesting that the formation of cavitations were nucleated under the tensile stress at high temperature rather than the evaporation of volatile species preexisted in the as-sintered ZS ceramics.

The stresses concentrated around the edge of cavitations are the possible reason for the formation of cracks. At a certain stress level, these cracks will propagate once the release of stored elastic energy induced by crack extension is equal to the energy for creation of two new fractural surfaces. So the cavitations are the main fracture initiation source of ZS ceramics at 1300–1600 °C.

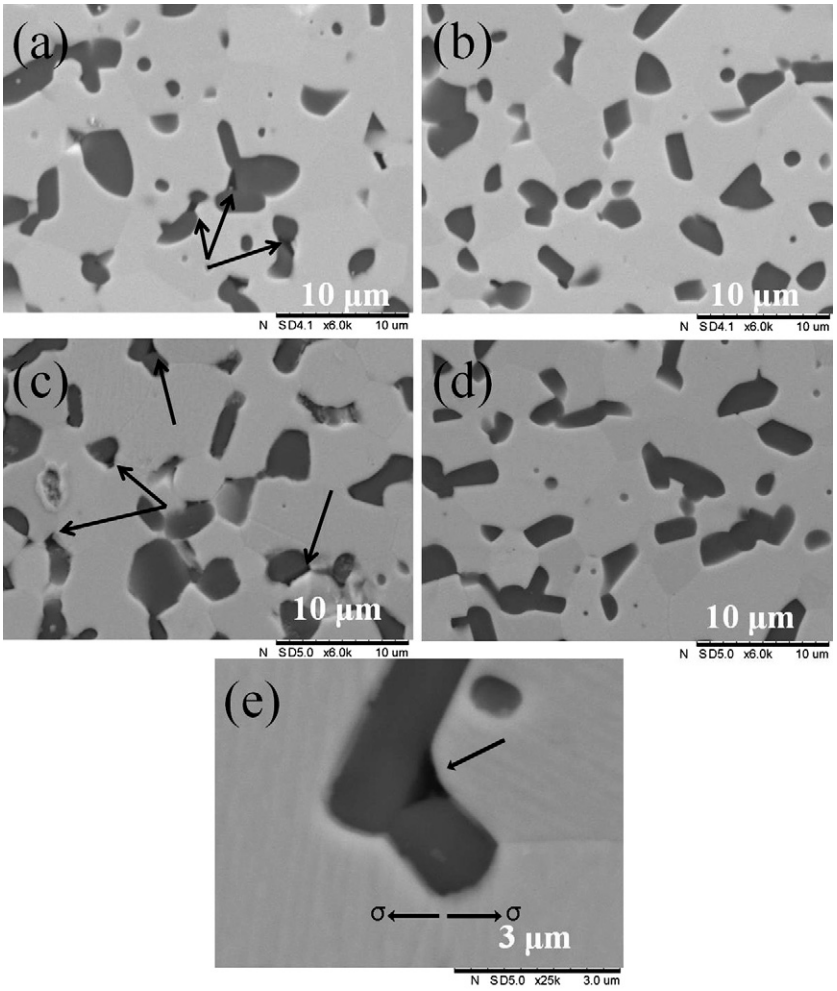

Fig. 7. Some typical micrographs on the tensile surfaces of ZS bars after high temperature bending tests observed by SEM. (a) and (b) were the sections near and far away from the fracture parts at 1300 °C, respectively. (c) and (d) were the sections near and far away from the fracture parts at 1600 °C, respectively. Cavitations were arrowed in these pictures. (f) was a high-magnification picture clearly shows the cavitations near the SiC/SiC/ZrB_2 triple junctions.

The degradation of bending strength of ZS in this temperature range should be attributed to the following reasons. (1) The grain boundary softening, i.e., the decrease of intergranular strength of ZS; (2) the formation of cavitations. When the test temperature was elevated from 1300 °C to 1600 °C, the characteristic of cavitations in both size and number were increased as shown in Fig. 7a and c. The growth of crack and coalescence of cavities will cause the formation of larger flaws; (3) grain sliding, as discussed below.

3.5. Grain sliding and internal friction

How did these cavitations nucleate during the high temperature test? Such cavitations are always observed on the tensile surface of crept samples, especially for particulate reinforced ceramics incorporated with secondary hard phase. Such as ZrO_2–20 wt% Al_2O_3[27] and Al_2O_3–17 vol% SiC.[28,29] In these samples, alumina and silicon carbide acted as the hard phases. It has been confirmed that cavities generated around the hard particles were a result of the grain boundary sliding of the matrix phase and the plunging of the hard particles. For hexagonal ZrB_2 and SiC, there are only two independent slip systems,[30] which were confined to the direction along the basal plane. The high stresses at the impingement of a single slip-band cannot be accommodated by homogeneous plastic deformation and hence a crack is nucleated or SiC particle is rotated, resulting in the formation of cavities, as described in Al_2O_3–SiC composites.[28,29] A similar phenomenon has recently been reported in the crept ZS samples,[31] which is considered as a result of the sliding of SiC and ZrB_2 grains under tensile stress. However, the specific mechanisms for the formation of cavitations in ZS ceramics during high temperature bending tests is still unclear, and will be investigated in future works.

Grain sliding in ceramics is always associated with grain boundary, e.g., grain boundary strength, impurities and segregation.[32] Firstly, due to the differences in the chemical compositions, the sliding mobility for ZrB_2/SiC grain boundary is expected to be higher than that of ZrB_2/ZrB_2, which is one reason for cavitations preferentially nucleated at ZrB_2/SiC/SiC triple junctions; secondly, as discussed in Section 3.1, compressive and tensile stresses are generated in the SiC and ZrB_2 grains during cooling from processing temperature, respectively. According to the results of Raman spectroscopy analysis, Watts et al. have reported the compressive stresses in the SiC particles to be as high as 810 MPa.[33] Furthermore, based on the stress value and the elastic parameters of SiC and ZrB_2, Watts calculated that stresses started to accumulate at approximately 1620 °C during cooling. Such residual stresses will relax when testing temperatures increased, i.e., SiC grains will not contract with adjacent ZrB_2 grains as tightly as at room temperature. The release of compressive stresses across the SiC grain boundaries at higher temperature will also accelerate their sliding mobility. Thirdly, though no thin amorphous films were observed at ZrB_2/SiC and ZrB_2/ZrB_2 grain boundary, small amounts of amorphous phases were detected as the impurities in ZS ceramics (Fig. 2b), and the effective role of these impurities on the grain sliding of ZS should also be considered. The wetting of grain boundary by such impurity segregations at high temperature should be another factor for grain sliding. These above assumptions were further proved by internal friction (Q^{-1}) investigation as plotted in Fig. 8.

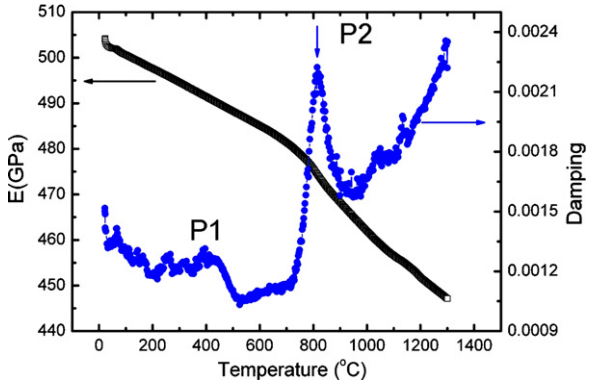

Fig. 8. Temperature dependence of Young's modulus and internal friction curve for ZS ceramics in argon atmosphere.

Internal friction is a powerful tool to analyze the grain boundary viscosity, the grain sliding, the dislocation behavior, and phase transformation in solid state materials at high temperature, since the position, magnitude and shape of internal friction peaks are the characteristics for materials.[34,35] Internal friction peak can also reflect the high temperature mechanical properties of the material indirectly, e.g., Schaller found damping peaks are sometimes related to the toughness increase of the material, as verified in WC-Co cermets and $ZrSiO_4$ ceramics.[36] Generally speaking, when the grains in ceramics are interlocked at triple point without any glass phase, the grain sliding was highly suppressed, so a relaxation Q^{-1} curve only shows an exponential-like background, e.g., high purity Sialon,[35] CVD BN[37] and direct-bonding $Zr_3Al_3C_5$[21]; when an amorphous film exists at the grain boundaries, a relaxation Q^{-1} peak will be superposed on the exponential-like background, resulting from the wetting of grain boundaries by amorphous phases, accompanied with grain sliding process, e.g., PLS $Zr_3Al_3C_5$.[21] The latter one is the feather in the present work (Fig. 8). The positions for damping peaks are always associated with the glass transition temperature (Tg) of the amorphous phase. Mirhadi has reported Tg of $CaO{\cdot}SiO_2{\cdot}ZrO_2$ glass is 773 °C,[38] approximately equal to the temperature of the main damping peak (P2) occurred in Fig. 8. Moreover, $CaO{\cdot}SiO_2{\cdot}ZrO_2$ glass phase was actually observed in the microstructure of ZS material (Fig. 2b), so the peak around 780 °C in Fig. 8 probably originated from the $CaO{\cdot}SiO_2{\cdot}ZrO_2$ phase. When temperature reached Tg, the viscosity of $CaO{\cdot}SiO_2{\cdot}ZrO_2$ phase decreased suddenly, so we propose it was another reason for accelerating the grain sliding of ZS ceramics.

Another weak peak was observed between 400 °C and 500 °C in the internal friction curve of ZS ceramics as marked in Fig. 8(P1). Since B_2O_3 has a transition temperature in the range from 450 °C to 500 °C, such peak (P1) has been considered as the softening of the amorphous B_2O_3 at the triple junctions.[39] Benefiting from the low oxygen contents in starting ZrB_2 powders and the B_2O_3 removing processes either by vacuum evaporation

or chemical reaction (reaction (I)), the remaining B_2O_3 in ZS ceramics was limited as indicated from internal friction analysis.

The grain boundary film viscosity (η) could be calculated from Fig. 8, by Eq. (1) and (2),[20,40] together with the elastic parameters of ZS ceramics (E, G and ν at room temperature are 504 GPa, 222 GPa and 0.138, respectively).

$$\eta = \frac{G_{LT}\delta}{2\pi f_{peak}\alpha(1-\nu)d} \quad (1)$$

where G_{LT} is the shear modulus at the low-temperature foot of the Q^{-1} peak. δ is the grain boundary film thickness, ν is the Poisson's ratio, d is the average grain size of ZS, and α is a grain morphology parameter. α can be calculated from the ratio of the unrelaxed G-modulus and the shear modulus G_{peak} at the Q^{-1} peak temperature according to Eq. (2).

$$\alpha = \frac{(G_{LT}/G_{peak}) - 1}{1-\nu} \quad (2)$$

If we assume grain boundary film thickness is 1 nm, the calculated η is 1.08×10^5 Pa s. This viscosity was comparable with SiC ceramics ($1.0–1.8 \times 10^5$ Pa s), and one order of magnitude higher than that from Si3N4 ceramics ($1.8–3.1 \times 10^4$ Pa s),[20] so the high temperature stiffness of ZS has not been seriously affected. The E-modulus of ZS decreases linearly with temperatures before and after damping peak (at 780 °C) occurred, while the slope of the latter is slightly larger than the former one. Benefiting from the low grain boundary film viscosity, at 1300 °C more than 88% of the room temperature E-modulus still was maintained, obviously higher than the value in the literature (~81%).[15]

4. Conclusions

Based on the investigation of the high temperature mechanical properties of ZrB_2–20 vol% SiC ceramics, the following conclusions can be drawn:

(1) The high temperature bend strength of ZS ceramics began to decrease above 1000 °C, while E-modulus decreases with the increase of the temperature. Its bend strength at 1600 °C is 460 ± 31 MPa and E-modulus at 1300 °C is 443.5 GPa, the corresponding strength and E modulus retention is 84% and 88%, respectively, these values are definitely higher than those in the literatures.

(2) Below 1000 °C, fracture of ZS ceramics mainly originate from the surface flaws induced by the machining process; above this temperature, the fracture sources changed to the cavitations or cracks near the SiC grains on the tensile surfaces of ZS. With increase of the temperatures, the facture mode of ZS also changed from transgranular to intergranular manner. Such transformation was easier to be observed on the tension side rather than the compression side, due to different status of stress distribution.

(3) The formation of cavitations and cracks near the SiC grains is considered to be grain sliding. Such grain sliding was accelerated by the impurity phases in ZS, which was also revealed by the relaxation peak from friction curve directly. The grain sliding is also a result of the relaxation of residual stresses across the SiC grain boundaries.

(4) Two typical damping peaks were found at the friction curve of ZS ceramics, and they originated from the oxygen impurities, e.g., B_2O_3 and ZrO_2–SiO_2–CaO based glass, respectively. When high purity ZrB_2 starting powders were chosen, the former peak could be highly suppressed while the latter one was still predominant.

(5) Degradation of high temperature strength and modulus of ZS ceramics could be associated with grain boundary softening and grain sliding, using high purity ZrB_2 powders as raw materials, the calculated grain boundary film viscosity in ZS was very high, so a high degree of strength and stiffness retention of ZS could be realized.

Acknowledgments

This work was financially supported by NSFC (No. 50632070 and 91026008), the bilateral project of NSFC-JSPS (No. 51111140017), the Research Fund of K.U.Leuven under project GOA/08/007. The Chinese Academy of Sciences Hundred Talents Program is gratefully acknowledged. Dr. Ji Zou thanks the Research Fund of K.U.Leuven for his post-doctoral F+/11/006 fellowship. Dr. Ji Zou also thanks Akhilesh Kumar Swarnakar for his great helpful in the discussion about IET.

References

1. Opeka M, Talmy IG, Wuchina EJ, Zaykoski JA, Causey SJ. Mechanical, thermal and oxidation properties of refractory hafnium and zirconium compounds. *J Eur Ceram Soc* 1999;**19**:2405–14.
2. Fahrenholtz WG, Hilmas GE. Refractory diborides of zirconium and hafnium. *J Am Ceram Soc* 2007;**90**:1347–64.
3. Rapp R. Materials for extreme environments. *Mater Today* 2006;**9**:6.
4. Zhang SC, Hilmas GE, Fahrenholtz WG. Pressureless densification of zirconium diboride with boron carbide additions. *J Am Ceram Soc* 2006;**89**:1544–50.
5. Zou J, Zhang G-J, Kan Y-M, Wang P-L. Pressureless densification of ZrB_2–SiC composites with vanadium carbide. *Scripta Mater* 2008;**59**:309–12.
6. Fahrenholtz WG, Hilmas GE, Zhang SC, Zhu SM. Pressureless sintering of zirconium diboride: particle size and additive effects. *J Am Ceram Soc* 2008;**91**:1398–404.
7. Zou J, Zhang G-J, Kan Y-M. Formation of tough interlocking microstructure in ZrB_2–SiC-based ultrahigh-temperature ceramics by pressureless sintering. *J Mater Res* 2009;**24**:2428–34.
8. Liu H-T, Zou J, Ni D-W, Wu W-W, Kan Y-M, Zhang G-J. Textured and platelet-reinforced ZrB_2-based ultra-high-temperature ceramics. *Scripta Mater* 2011;**65**:37–40.
9. Sciti D, Guicciardi S, Silvestroni L. SiC chopped fibers reinforced ZrB_2: effect of the sintering aid. *Scripta Mater* 2011;**64**:769–72.
10. Parthasarathy TA, Rapp RA, Opeka M, Kerans RJ. A model for the oxidation of ZrB_2, HfB_2 and TiB_2. *Acta Mater* 2007;**55**:5999–6010.
11. Fahrenholtz WG. Thermodynamic analysis of ZrB_2–SiC oxidation: formation of a SiC-depleted region. *J Am Ceram Soc* 2007;**90**:143–8.
12. Zhang SC, Hilmas GE, Fahrenholtz WG. Mechanical properties of sintered ZrB_2–SiC ceramics. *J Eur Ceram Soc* 2011;**31**:893–901.
13. Zimmermann JW, Hilmas GE, Fahrenholtz WG. Thermo-physical properties of ZrB_2 and ZrB_2–SiC ceramics. *J Am Ceram Soc* 2008;**91**:1405–11.
14. Loehman R, Corral E, Dumm HP, Kotula P, Tandon R. Ultra high temperature ceramics for hypersonic vehicle applications, Sandia Report Sand 2006-2925, 2006.

15. Gasch MJ, Ellerby DT, Johnson SM. Ultra high temperature ceramic composites. In: Narottal P, Bansal, editors. *Handbook of ceramic composites*. Kluwer Academic Publishers; 2005. p. 212–4.
16. Bellosi A, Monteverde F, Sciti D. Fast densification of ultra-high temperature ceramics by spark plasma sintering. *Int J Appl Ceram Technol* 2006;**3**: 32–40.
17. Hu P, Wang Z. Flexural strength and fracture behavior of ZrB_2–SiC ultra-high temperature ceramic composites at 1800 °C. *J Eur Ceram Soc* 2010;**30**:1021–6.
18. Ni DW, Zhang GJ, Kan YM, Wang PL. Synthesis of monodispersed fine hafnium diboride powders using carbo/borothermal reduction of hafnium dioxide. *J Am Ceram Soc* 2008;**91**:2709–12.
19. Zou J, Zhang GJ, Kan YM, Wang PL. Hot-pressed ZrB_2–SiC ceramics with VC addition: chemical reactions, microstructures, and mechanical properties. *J Am Ceram Soc* 2009;**92**:2838–46.
20. Roebben G, Duan R-G, Sciti D, Van der Biest O. Assessment of the high temperature elastic and damping properties of silicon nitrides and carbides with the impulse excitation technique. *J Eur Ceram Soc* 2002;**22**:2501–9.
21. He LF, Lu XP, Bao YW, Wang JY, Zhou YC. High-temperature internal friction, stiffness and strength of Zr–Al (Si)–C ceramics. *Scripta Mater* 2009;**61**:60–3.
22. Monteverde F, Bellosi A. Effect of the addition of silicon nitride on sintering behavior and microstructure of zirconium diboride. *Scripta Mater* 2002;**46**:223–8.
23. Zhang GJ, Deng ZY, Kondo N, Yang JF, Ohji T. Reactive hot pressing of ZrB_2–SiC composites. *J Am Ceram Soc* 2000;**83**:2330–2.
24. Larsen DC, Adams JW, Bcrtz SA, Ruh R. Evidence of strength degradation by subcritical crack growth in Si_3N_4 and SiC. In: Bradt RC, Evans AG, Hasselman DPH, Lange FF, editors. *Fracture mechanism of ceramic*. New York: Plenum; 1983. p. 571.
25. Kim YW, Chun YS, Nishimura T, Mitomo M, Lee YH. High-temperature strength of silicon carbide ceramics sintered with rare-earth oxide and aluminum nitride. *Acta Mater* 2007;**55**:727–36.
26. Kalish D, Clougherty EV, Kreder K. Strength, fracture mode, and thermal stress resistance of HfB_2 and ZrB_2. *J Am Ceram Soc* 1969;**52**:30–6.
27. Owen DM, Chokshi AH, Nutt SR. Nucleation and growth characteristics of cavities during the early stages of tensile creep deformation in a superplastic zirconia–20 wt% alumina composite. *J Am Ceram Soc* 1997;**80**:2433–6.
28. Ohji T, Nakahira A, Hirano T, Niihara K. Tensile creep behavior of alumina/silicon carbide nanocomposite. *J Am Ceram Soc* 1994;**77**:3259–62.
29. Ohji T, Yamauchi Y. Diffusional crack growth and creep rupture of silicon carbide doped with alumina. *J Am Ceram Soc* 1994;**77**:678–82.
30. Haggerty JS, Lee DW. Plastic deformation of ZrB_2 single crystals. *J Am Ceram Soc* 1971;**54**:572–6.
31. Guo W-M, Zhang G-J, Lin H-T. High-temperature flexural creep of ZrB_2–SiC ceramics in argon atmosphere. *Ceram Int* 2012;**38**:831–5.
32. Kinoshita T, Munekawa S, Tanaka SI. Effect of grain boundary segregation on high temperature strength of hot-pressed silicon carbide. *Acta Mater* 1997;**45**:801–9.
33. Watts J, Hilmas G, Fahrenholtz WG, Brown D, Clausen B. Stress measurements in ZrB_2–SiC composites using Raman spectroscopy and neutron diffraction. *J Eur Ceram Soc* 2010;**30**:2165–71.
34. Nowick AS, Berry BS. *An elastic relaxation in crystalline solids*. New York: Academic Press; 1972. p. 1–2.
35. Pezzotti G, Kleebe HJ, Okamoto K, Ota K. Structure and viscosity of grain boundary in high-purity Sialon ceramics. *J Am Ceram Soc* 2000;**83**:2549–55.
36. Schaller R. Mechanical spectroscopy of the high-temperature brittle-to-ductile transition in ceramics and cermets. *J Alloys Compd* 2000;**310**:7–15.
37. Pezzotti G, Kleebe HJ, Ota K, Nishida T. Viscoelastic sliding and diffusive relaxation along grain boundaries in polycrystalline boron nitride. *Acta Mater* 1997;**45**:4171–9.
38. Mirhadi B, Mehdikhani B. Crystallization behavior and microstructure of $(CaO{\cdot}ZrO_2{\cdot}SiO_2)$–$Cr_2O_3$ based glasses. *J Non-Cryst Solids* 2011;**357**:3711–6.
39. Herrmann M, Swarnakar AK, Thiele M, Van der Biest O, Sigalas I. High temperature properties of B_6O-materials. *J Eur Ceram Soc* 2011;**31**:2387–92.
40. Mosher DR, Raj R. Use of the internal friction technique to measure rates of grain boundary sliding. *Acta Metall* 1974;**22**:1469–74.